# Experimental implementation of a Quality-by-Control (QbC) framework using a mechanistic PBM-based nonlinear model predictive control involving chord length distribution measurement for the batch cooling crystallization of L-ascorbic acid

Botond Szilágyi[1,2,3], Ákos Borsos[1], Kanjakha Pal[2], Zoltán K. Nagy[1,2*]

[1]*Department of Chemical Engineering, Loughborough University, Leicestershire, Loughborough Le11 3TU, United Kingdom,*

[2]*School of Chemical Engineering, Purdue University, West Lafayette 47907-2100, USA,*

[3]*Department of Chemical Engineering, "Babes-Bolyai" University, Arany Janos Street 1, Cluj Napoca 400028, Romania*

**zknagy@purdue.edu, z.k.nagy@lboro.ac.uk*

***Abstract***

L-ascorbic acid is synthetized in large industrial scale from glucose and marketed as an immune system strengthening agent and anti-oxidant ingredient. The overall yield of conversion of the precursor glucose to L-ascorbic acid is limited, therefore the crystallization is a critically important step of the L-ascorbic acid production from economic point of view. It is widely accepted that the crystal size distribution (CSD) influences numerous relevant macroscopic properties of the final crystalline product and it also significantly affects the downstream operations. The present paper discusses the chord length distribution (CLD, which is directly related to the CSD) control, during the crystallization of L-ascorbic acid from aqueous solution. Batch crystallization process is

employed, which is the classical, and still dominant, operation in fine chemical and pharmaceutical industries. A comparative experimental study of two state-of-the-art Quality-by-Control (QbC) based crystallization design approaches are presented: (1) a model-free QbC based on direct nucleation control (DNC) and (2) a model-based QbC using a novel nonlinear model predicative control (NMPC) framework. In the first investigation, the DNC, a process analytical technology based state-of-the-art model free control strategy, is applied. Although, DNC requires minimal preliminary system information and often provides robust process control, due to the unusual crystallization behavior of L-ascorbic acid, it leads to long batch times and oscillatory operation. In a second study the benefits of model-based QbC approach are demonstrated, based on using a NMPC approach. A population balance based crystallization process model is built and calibrated by estimating the nucleation and growth kinetics from concentration and CLD measurements. A projection based CSD to CLD forward transformation is used in the estimation of nucleation and growth kinetics. For robustness and adaptive behavior, the NMPC is coupled with a growing horizon state estimator, which is aimed to continuously improve the model by re-adjusting the kinetic constants. The study demonstrates that the model-based QbC framework can lead to rapid and robust crystallization process development with the NMPC system presenting good control behavior under significant plant model mismatch (PMM) conditions.

**Keywords**: ascorbic acid, kinetic estimation, DNC, population balances, NMPC, Quality-by-Control, QbC

## *Introduction*

L-ascorbic acid (AA), often called as vitamin C, was extracted from paprika. It is a very potent anti-oxidant effect which leads to increased metabolic flux in the Krebs cycle which strengthens the immunological system (Berg et al., 2010). Since extraction of L-ascorbic acid from natural sources is not cost-effective, it is synthetized at industrial scale through a biotechnological route from glucose with an estimated worldwide production rate of 110 metric kilotons. AA is used as an ingredient in the pharmaceutical industry (50 %), food industry (25 %), beverage sector (15 %) and for animal feed uses (Pappenberger and Hohmann, 2014). The overall yield for the glucose transformation to L-ascorbic acid is between 50-60 % thus it is important to reduce the separation and purification losses (Wierzbowska et al., 2011). Since L-ascorbic acid is mainly marketed in solid crystalline form, the particle formation step is very important since the CSD influences numerous macroscopic material properties, such as dissolution rate and mechanical properties (Myerson, 2002). In the production of L-ascorbic acid, crystallization takes the critical role of simultaneously being the purification as well as the particle formation stage. The separation and purification of L-ascorbic acid has been investigated intensively (Beuzelin-Ollivier et al., 2012) and this paper focuses on controlling the CSD during crystallization.

The state-of-the-art control strategies of cooling crystallizers can be divided into two major groups: model free and model based control approaches (Nagy et al., 2013). Direct nucleation control (DNC) is a model free control method, which controls the crystal size through the relative solution crystal number density *via* repeated and controlled dissolution-growth (heating-cooling) stages (Abu Bakar et al., 2009).Supersaturation control (SSC) is another model free control strategy, which is based on the principle that the crystallization process should be conducted in the metastable zone to suppress nucleation (Nagy and Braatz, 2012). These two well established control strategies have found numerous applications, both as solo control strategies (Barrett et al., 2010; Kacker et al., 2016) as well as combined control approach (Griffin et al., 2015)

Model based control techniques use real time simulation based on a process model to predict the effects of inputs and disturbances on the systemic output. In essence this translates to real time optimization of the control signal, which in the case of cooling crystallization translates into the prediction of the future temperature profile (Moldoványi et al., 2005; Qin and Badgwell, 2000). The basic requirement of a model based controller is the existence of an adequate process model in terms of complexity, accuracy and solution time (Agachi et al., 2007). The population balance (PB) framework is the most widely accepted modeling approach in the mathematical description of crystallization processes (Hulburt and Katz, 1964). The PB equations, from mathematical point of view, are hyperbolic partial differential equations (PDEs), which becomes an integro-PDE, if agglomeration and/or breakage is also considered. Due to the inherent complexity of these equations, the solution might become complicated, inaccurate and time consuming. Numerous mathematical and numerical techniques have been addressed to the solution of PB equations (PBEs). Moment based methods (Randolph and Larson, 1973) and their quadrature extensions (McGraw, 1997) are computationally efficient, accurate and widely applicable techniques (Grosch

et al., 2007) to calculate the moments of distribution. A major problem with these methods is that the estimation of CSD based on its moments is not exact thereby limiting their applicability. In contrast, the combined method of moments and method of characteristics(MOM-MOC) is able to accurately solve the PBE with nucleation and growth with reduced computational burden (Aamir et al., 2009). However, when nucleation is also modeled using the PBEs, more adaptations becomes necessary using MOM-MOC which also makes it practically infeasible as a solution procedure (Mesbah et al., 2009). High resolution finite volume method (HR-FVM) is a solution technique of hyperbolic PDEs (LeVeque, 2002), providing a generic framework for the numerical simulation of PBEs even in multiple dimensions (Gunawan et al., 2004). FVM is a discretization based technique: finer discretization entails higher accuracy but this also translates into higher computational costs. Significant reduction in the time to solve PBEs based on FVM can be achieved by efficient computer implementation (Majumder et al., 2010; Szilágyi and Nagy, 2016).

The vast majority of literature reports controlling crystallization using underlying optimization based strategies employ moment based PBE solution (Acevedo et al., 2015; Bötschi et al., 2018; Paz Suárez et al., 2011; Su et al., 2017; Zhang and Rohani, 2004). However, a full PBE based approach would enable the direct manipulation of CSD, instead of only its moments. Moreover, to use the valuable distributional information of the CLD, the calculation of the CSD would be required, but in the field of control applications the literature is meager (Ma and Wang, 2012; Mesbah et al., 2012). A major limitation of real time full PBM based control is the difficulty of the state estimation, since the actual CSD is required as the initial condition of the process optimization and simulations (in addition to the increased computational time). Since the CSD cannot be accurately measured with on-line tools, it has to be estimated through state estimation using the measurable data (Porru and Özkan, 2017; Szilagyi et al., 2018). The state estimator is

also required for robust control (Nagy and Braatz, 2003; Rawlings and Mayne, 2012) and it represent a crucial part of the predictive control system (Mesbah et al., 2011b). To the best of the authors knowledge, the experimental implementation of an NMPC system that uses the CLD as direct feedback information was not reported in the literature before.

Even though the crystallization modeling and control is an intensively investigated topic and the fact L-ascorbic acid is an industrially important product produced in large quantities, only a few papers deal with its crystallization. Eggers et al. investigated the shape and size variations during L-ascorbic acid crystallization using state-of-the-art process analytical technology (PAT) tools assuming two dimensional crystal shape (Eggers et al., 2009). Wierzbowska et al. investigated the solubility, nucleation and growth kinetics have been investigated for ethanol-water systems (Shalmashi and Eliassi, 2008; B. Wierzbowska et al., 2008; Bogusława Wierzbowska et al., 2008). In a theoretical investigation it was shown that the shape of L-ascorbic acid exhibits complex habit changes during the crystallization (Uesaka and Kobayashi, 2002). However, a control oriented study on L-ascorbic acid crystallization has not been published yet.

Quality-by-Control (QbC) has been proposed recently as a novel paradigm to design processes, whereby feedback control is used to obtain suitable operating procedures by direct adaptation of the operating conditions during the process using a feedback control based approach; hence, it provides a much faster methodology to find the optimal operating procedure, requiring less material as traditional Quality-by-Design (QbD) approaches based on standard design-of-experiments techniques (Simone at al., 2015; Yang and Nagy, 2015).

The aim of the current work is to provide and experimental proof-of-concept and comparison between two state-of-the-art QbC frameworks: (i) a model-free QbC, based on direct nucleation

control (DNC), which is one of the most advanced model-free control strategies and (ii) a model-based QbC using a full PBM based nonlinear model predictive control (NMPC), which is one of the most complex model based control approaches. These approaches are implemented and investigated for the cooling batch crystallization of L-ascorbic acid from aqueous solutions, used as the model system with large industrial significance, however the methodology presented is generic and applicable for most batch cooling crystallization processes. For the model system, a kinetic investigation has also been carried out to estimate the nucleation and growth kinetics based on concentration and CLD measurements, which is then used in the NMPC. It was shown that the system is characterized by a large time delay to time constant ratio with the particular crystallization kinetics, which causes the DNC to oscillate. However, the NMPC approach produced good quality crystals with significantly better CSD than the corresponding linear cooling, and with considerably shorter batch time than the DNC. This work provides an exemplary case study for the comprehensive experimental implementation and investigation of a high-resolution finite volume PBM based NMPC with the novel features of using real-time kinetic parameter adaptation through a growing horizon estimation and applying direct CLD measurement and FBRM sensor model with a forward CSD to CLD conversion. The proposed framework also provides a simultaneous model identification and kinetic parameter refinement as well as optimal model based temperature design approach through a single batch experiment, offering a platform for rapid and automated model identification and model based optimal design for batch cooling crystallization systems.

***Direct nucleation control of L-ascorbic acid crystallization***

The main idea of DNC is to keep the relative particle number between some pre-defined limits while the system is gradually cooled to the desired final temperature. For a predefined difference

between the initial and final temperatures, the produced crystal number is inversely proportional with the mean crystal size. The actual crystal number density in solution, however cannot be directly measured but a relative particle number can be tracked, traditionally with Focused Beam Reflectance Measurement (FBRM) (Saleemi et al., 2012), and more recently also with in-line imaging techniques (Borsos et al., 2017). Increase of FBRM counts generally result from nucleation while decrease in counts results from dissolution. Consequently, the DNC heats up the crystallizer if the upper count limit is exceeded and cools otherwise. The major advantage of DNC is that it requires no preliminary system information such as the solubility/nucleation curves or crystallization kinetics, as these boundaries of the operating zone are automatically detected during the actual process operation.

For the DNC experiments 500 g saturated (at 35 ºC) L-ascorbic acid (99 %, Fisher Scientific) solution was prepared and introduced into a 1 L jacketed glass crystallizer. The stirring rate of 400 RPM provided a good tradeoff between having good mixing and a low breakage rate. During the experiments the relative crystal number was tracked with FBRM (iC FBRM, V4.3.377). For the DNC, the lower and upper count limits were set to 1600 and 1800 counts/s, while the heating and cooling rates were set to 0.05 ºC/min because further decrease in cooling rate might lead to excessive batch time. In the first stage, the system was heated up to 45 ºC for complete dissolution. Then, the crystallizer was cooled to 34 ºC and a low pre-measured quantity of seed was added to promote nucleation; this was the starting point of DNC. Crystallization Process Informatics System (CryPRINS or CryMOCO), an in-house developed crystallization monitoring and control software, was used for the implementation of the DNC.

In Figure 1, it can be seen that DNC did not converge to the desired final temperature (20 ºC) but instead the temperature oscillates in time, which can be explained by the particular crystallization

kinetics of the L-ascorbic acid system. Ascorbic acid has a very broad primary nucleation zone width (often around 35 ºC sub-cooling). If seeded at such high supersaturation, instantaneous secondary nucleation occurs, but at low supersaturation the secondary nucleation rate is very low. The growth rate is also relatively low for this system leading to slow consumption of solution supersaturation. These two kinetic properties inherently introduce an apparent dead time in the FBRM counts, which leads to oscillatory DNC behavior. After 60 hours the system enters into an oscillatory regime with constant amplitude, with the temperature varying between 21 and 25 ºC. The counts are kept between 1500 and 2000, while the mean chord lengths oscillate around 15 µm. It should be noted that setting higher desired final temperature, the system might be able to converge. However, higher final temperature leads to a loss in process yield and hence is not desirable.

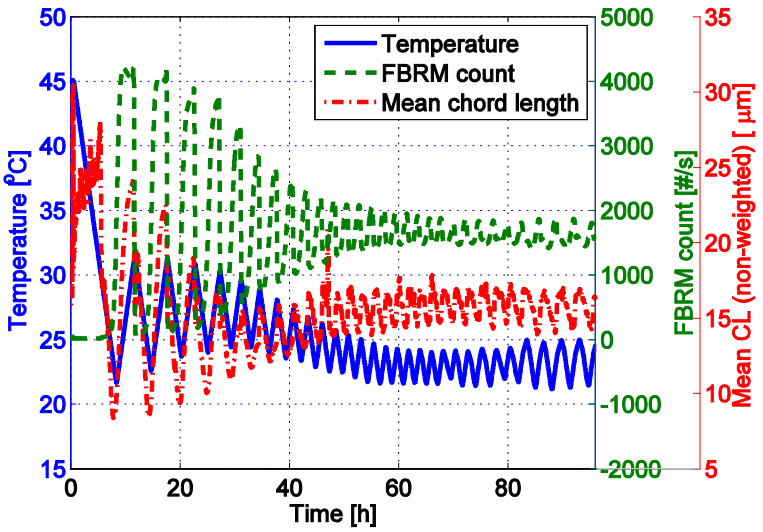


**Figure 1**. The variation of controlled (FBRM counts/s) and manipulated (temperature) variables as well as the mean CL during the DNC experiments.

Figure 2 shows the PVM images of crystals during the sustained oscillations (between 60 and 96 hours from Figure 1). The images illustrate that the CSD is wide, although the fines could be removed from the product by a partial dissolution, which can improve the CSD uniformity.

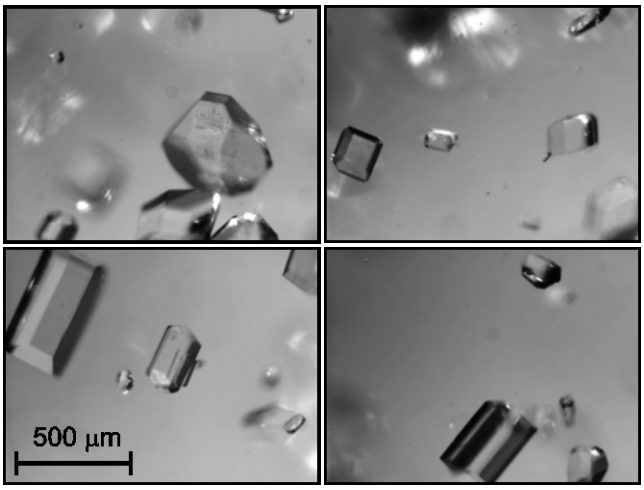


**Figure 2**. L-ascorbic acid crystals obtained from the 4 day long DNC batch of Figure 1, taken during the final period of the batch (80-90 h).

Based on the results, the system required 60 hours to enter in "constant oscillations", which can be considered too long from a practical application point of view. The number of heating stages could be reduced by applying slower cooling, which would give more time for the crystals to growth, but slow cooling would lead to excessive batch time, which makes it also infeasible.

According to the investigations, the apparent time delay caused by the nucleation kinetics, poses unforeseen challenges for the DNC controller. Generally, systems characterized by a large time delay to time constant ratio, require predictive controllers, thus in this case an NMPC is expected to give improved control performance.

## *Modeling and model identification of L-ascorbic acid crystallization*

*Model development*

A key requirement of the model based controller is the existence of an adequate process model, which can be solved computationally much faster than the time scale of the actual process evolution, thus enabling real time optimization. The trade-off among model complexity, dimensionality and solution accuracy are all dictated by the objectives of the NMPC system. Thus, the control-relevant model used in the NMPC is not necessarily the most comprehensive model, which should be used for fundamental system analysis.

The shape of L-ascorbic acid varies during its crystallization from water. In this study, since a 1D PBM is used the crystals are considered to have cubic shape, characterized with a single dimension, the edge length ($L$). According to the observed system behavior during the DNC experiments, secondary nucleation and size dependent growth mechanisms dominate throughout the process thus these will be included into the PBM. In order to take full advantage of the distributional information provided by the FBRM, a full discretization based PBM solution is required thus the computationally efficient moment based methods are not applicable. Instead, the HR-FVM is used to solve the model equations. To summarize, the characteristics of the adequate process model are:

- One dimensional PBM assuming cube-like shape
- Secondary nucleation and size dependent growth mechanisms
- Fast and accurate numerical solution of the PBE with nucleation and size dependent growth

For the characterization of particle population the univariable size density function *n(L,t)dL,* is defined, which gives the number of crystals within the *(L, L+dL)* size domain at time *t*. Assuming perfect mixing at all length scales and homogeneous suspension temperature field, the PBE, governing the temporal evolution of the size density function takes the form (Randolph and Larson, 1973):

$$\frac{\partial n(L,t)}{\partial t} + \frac{\partial [G(\sigma,T,L)n(L,t)]}{\partial L} = B(\sigma,T)\delta(L-L_n) \tag{1}$$

with the initial and boundary conditions:

$$n(L,0) = n_0(L)$$
$$\lim_{L\to\infty} n(L,t) = 0 \tag{2}$$

In Eq.(1) the first term describes the temporal evolution of the size density function, the second term stands for the crystal growth, while the right hand side takes into consideration the nucleation, assuming constant nucleon size of $L_n$.

Secondary nucleation is considered, given by the temperature dependent power-law equation (Mersmann, 2001):

$$B(\sigma,T) = k_b \sigma^b V_C^j exp\left[-\frac{E_b}{RT}\right] \tag{3}$$

where $\sigma$ denotes the relative supersaturation:

$$\sigma = \frac{c}{c_s(T)} - 1 \tag{4}$$

and $V_C$ represents the total volume of crystal population, expressed by the integral:

$$V_C = \int_0^{\infty} L^3 n(L,t) dL \tag{5}$$

The solubility of ascorbic acid can be described as a function of temperature by the power law equation (Eggers et al., 2009):

$$c_s(T) = p_1 + p_2 T + p_3 T^2 \tag{6}$$

The growth rate, after the experimental observations, is described by a size, supersaturation and temperature dependent rate function (Mersmann, 2001):

$$G(\sigma, T, L) = k_G \sigma^g L^\gamma exp\left[-\frac{E_g}{RT}\right] \tag{7}$$

The macroscopic mass balance for the solute concentration takes the form:

$$\frac{dc}{dt} = -\rho_c \left[3 \int_0^{L_{max}} G(\sigma, T, L) L^2 n(L,t) dL + B(\sigma, T) L_n^3\right] \tag{8}$$

with $c(0) = c_0$ initial condition.

As the temperature is the manipulated variable, energy balance is not required for model closure, assuming the solution is well mixed and the temperature field inside the reactor is spatially uniform. In summary, the batch crystallizer dynamics is described by the set of partial and ordinary differential equations (1) - (8) with the corresponding kinetic and thermodynamic equations.

The model equations were solved using the HR-FVM. For brevity, the numerical solution and implementation approach is not given here, but can be found in the literature (Gunawan et al.,

2004), 21]. Based on the experimental observation, in the model solution the 0-1000 μm crystal size domain was applied. Uniformly distributed mesh was used with N = 1000 elements, which ensured the high-fidelity model solution. The *crysiv* MATLAB based function was used to solve the model equations (Szilágyi and Nagy, 2016). The material related constants are listed in Table 1.

**Table 1.** Material related constants of L-ascorbic acid crystallization.

| Parameter | Name | Value, U.M. |
|---|---|---|
| $p_1$ | Solubility constant | 0.1416, kg kg$^{-1}$ |
| $p_2$ | Solubility constant | 3.37 10$^{-3}$, kg kg$^{-1}$ $^{o}$C$^{-1}$ |
| $p_3$ | Solubility constant | 4.02 10$^{-5}$, kg kg$^{-1}$ $^{o}$C$^{-2}$ |
| $\rho_c$ | Crystal density | 1650 kg m$^{-3}$ |
| $L_n$ | Size of nuclei (lower bound of discrete CSD domain) | 10$^{-6}$ m |

The constants of nucleation and growth rate equations have not been determined yet, therefore these kinetic parameters must be estimated.

*Experimental setup and procedure*

The model parameter estimation was performed based on concentration and CLD measurement data obtained from experiments. The solutions, 500 g for each experiment, were prepared from distilled water and L-ascorbic acid (>99 %, Fisher Scientific). A jacketed glass crystallizer was used, which was linked to a Huber (Ministat 230) thermo-regulator. A three-blade impeller

agitator, operated at 350 rot/min was used, ensuring a well-mixing suspension. The final temperature was 20 ºC in all four experiments. The rest of the conditions are listed in Table 2.

**Table 2.** Conditions of the model identification experiments.

| No | Saturation temp. (ºC) | Seeding temp. (ºC) | Seed volume frac. (-) | Batch time (h) |
|---|---|---|---|---|
| 1 | 34.5 | 33.0 | $3.0 \times 10^{-3}$ | 5 |
| 2 | 34.5 | 34.5 | $1.0 \times 10^{-3}$ | 15 |
| 3 | 30 | 29.5 | $0.6 \times 10^{-3}$ | 23 |
| 4 | 30 | 30.0 | $1.5 \times 10^{-3}$ | 8 |

The experimental conditions were designed to be considerably different, in order to mitigate correlation between the estimated kinetic constants. In the model identification experiments, the seed generation method described in the literature was used (Eggers et al., 2009). The seeds were added in the form of suspension.

During the crystallization, the solute concentration was tracked with an on-line UV-VIS spectrophotometer (Zeiss MCS621 UV-VIS), following the 275 nm peak. The quick calibration method was used: 500 g solution, saturated at 31 ºC, was prepared and kept at 20 ºC until reaching the saturation concentration. Then the solution was slowly heated to 35 ºC and kept for 60 minutes to ensure complete dissolution, which was followed by slow cooling. During the slow heating period, the solution concentration followed the solubility curve due to very slow solute dissolution,

whereas during the slow cooling phase it was constant since primary nucleation did not occur. The following non-linear temperature and absorbance (A) dependent calibration equation was used:

$$c = p_{00} + p_{10}A + p_{20}A^2 + p_{01}T + p_{02}T^2 + p_{11}AT \quad (9)$$

The parameters of Eq.(9) were estimated from the results of the calibration experiment by formulating and solving a nonlinear least square optimization problem. The optimization was carried out in MALAB R2015b and the resulted parameters are listed in Table 3.

**Table 3.** Optimal calibration parameters of the on-line ATR-UV-Vis spectrophotometer for the concentration of L-ascorbic acid in water.

| $p_{00}$ | $p_{10}$ | $p_{20}$ | $p_{01}$ | $p_{02}$ | $p_{11}$ |
|---|---|---|---|---|---|
| $3.64\times10^{-1}$ | -1.67 | 2.31 | $2.13\times10^{-2}$ | $-3.02\times10^{-5}$ | $-2.96\times10^{-2}$ |

The results of the UV calibration experiment are illustrated in Figure 3, indicating that good agreement exists between the measured (solubility) and calibrated concentrations. Thus, the calibration Eq.(9) can be used in the model parameter estimation.

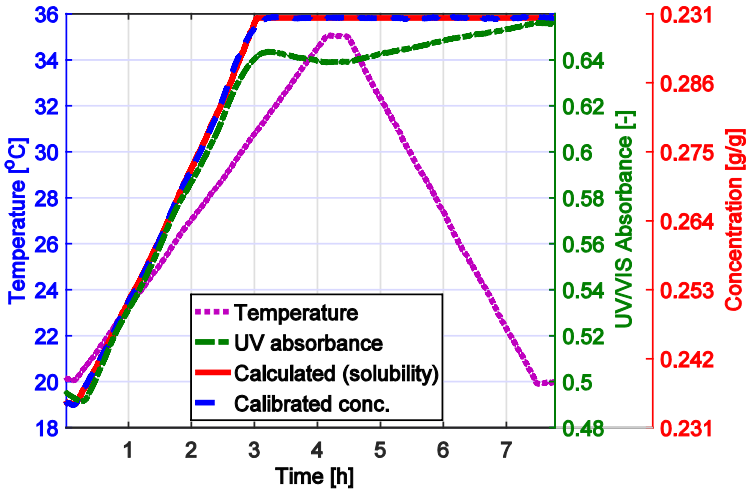


**Figure 3.** Results of the quick calibration experiment for concentration measurement with the ATR-UV/VIS spectrophotometer.

The numerical solution of the PBE, given by Eq.(1), provides the temporal evolution of the CSD. To compare it with the measured CLD, a suitable transformation of the CSD into the CLD, or vice-versa, is needed. The CSD to CLD transformation has been extensively researched over the past three decades and several methods have been proposed, however none of these is exact (Agimelen et al., 2015; Hukkanen and Braatz, 2003; Kail et al., 2009; Li et al., 2006; Worlitschek et al., 2005). All methods proposed suffer from the ill-conditioned structure of the inverse transformation and only work under very specific experimental conditions and system specifications. Recently, a novel formulation of the geometrical modeling approach was proposed to predict the CLD from the CSD, rather than doing traditional inverse transformation of the CLD to CSD. This approach practically simulates what the FBRM measures, providing a mechanistic FBRM sensor model, and does not suffer from ill-conditioning. Using efficient implementation, the proposed CSD to CLD forward transformation is applicable in real time, hence it can be used in model predictive control

approaches. The approach is briefly described here, for more detailed description please refer to the literature (Szilagyi et al., 2018). Essentially, the transformation has two major steps:

- Calculation of the CLD of a single crystal (with assumed shape; e.g. cubic in this study) by mapping all possible chord lengths (approximated by straight line) of all possible 2D projections. The CLDs of the individual crystals are pre-computed for all crystal length used in the HR-FVM solution. Such a simulation is presented for an L = 100 μm crystal in Figure 4a. The CLD maximum is at CL~105 μm, as there are numerous longer diagonals than the edge length.
- The overall CLD is computed by summing up the individual crystal CLDs for the calculated CSD, using the weighted sum of individual CLDs (see Figure 4b). The figure depicts the situation, when the CLDs are weighted by the number of crystals of a given size provided by the CSD. This means that the contribution of a crystal population to the overall CLD depends on the number of crystals of the respective size in the particular population. However, the larger crystals are measured with higher probability by the FBRM. To take this into account in addition to the crystal number, the mean projection area should also be used as a weighting factor (Worlitschek et al., 2005). According to Figure 4b, differences exist more likely in the lower CL domain. In this work, the PBM is combined with the FBRM sensor model that uses the forward CSD to CLD prediction based on the number and projection area based weighted CLD, hence the output of the simulation model is the CLD distribution that can be directly compared with the FBRM measurements. Note that this transformation is not meant to be accurate as an absolute CSD to CLD transformation, as it is optimized for real-time feasibility for feedback control applications, and by combining it with an error estimation algorithm during its application,

the overall control system can cope with errors in the CSD to CLD transformation that can result from different practical limitations, such as variations in the refractive index of the crystals, or variation in the difference of refractive index of crystals and solution, preferential orientation or imperfect mixing. These will become factors that contribute to the overall model-plant mismatch in the algorithm and the adaptive feature of the control approach, conveyed by the periodic re-estimation of the model parameters by a growing horizon estimation, incorporates these effects in the error model.

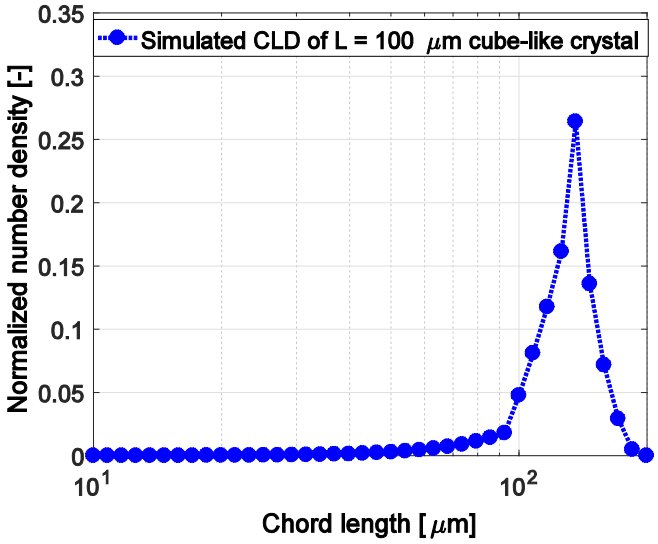


a)

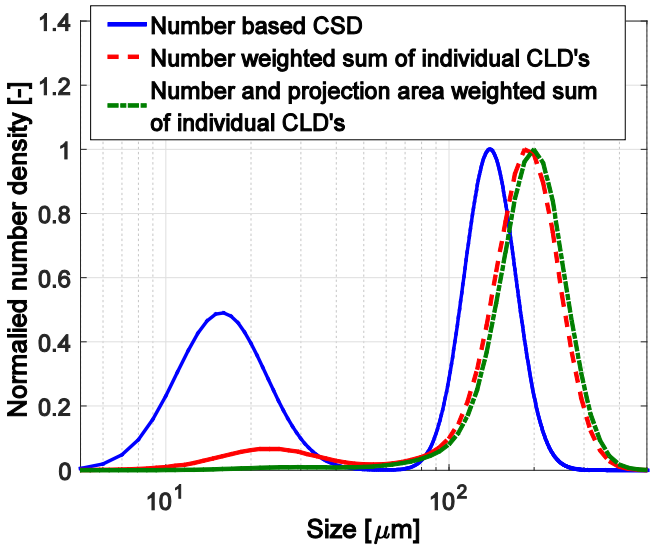


b)

**Figure 4.** a) Simulated CLD of a cubic crystal with edge length of L = 100 µm; and b) illustration of the CSD to CLD forward transformation using number weighted and number and projection area weighted CLD calculation.

*Model parameter estimation*

In the simulation the initial CSD was calculated from the initially measured CLD by solving the inverse of the CSD to CLD forward transformation, formulated as an optimization problem, to find the CSD, which has a simulated CLD that approximates best the measured CLD. The decision variables in the optimization were the discrete number based seed distribution ($CSD_{s,i}^{nb}$). The following sum-squared error (SSE) based objective function was minimized in the optimization:

$$SSE(CSD_s^{nb}) = \sum_{i=1}^{M}\left[\left(CL_{i,m}^{nw} - CL_{i,s}^{nw}\right)^2 + w_1\left(CL_{i,m}^{sqw} - CL_{i,s}^{sqw}\right)^2\right] + \sum_{i=1}^{N-1}\left[w_2\left(\frac{CSD_{s,i+1}^{nb} - CSD_{s,i}^{nb}}{\sum_{i=1}^{N} CSD_{s,i}^{nb}}\right)^2 + w_3\left(\frac{CSD_{s,i+1}^{vb} - CSD_{s,i}^{vb}}{\sum_{i=1}^{N} CSD_{s,i}^{vb}}\right)^2\right] \stackrel{!}{=} min \quad (10)$$

The first part of Eq.(10) is fits the simulated unweighted and square-weighted CLs ($CL_{i,s}^{nw}$ and $CL_{i,s}^{sqw}$) to the measured data ($CL_{i,m}^{nw}$ and $CL_{i,m}^{sqw}$) at every CL bin ($M$). The second part ensures smooth variation of the number ($CSD_{s,i}^{nb}$) and volume ($CSD_{s,i}^{vb}$) based seed distributions at every discrete crystal size bin ($N$). The optimization was solved in MATLAB R2015b, using an evolutionary global optimization algorithm with covariance matrix adaptation (CMA-ES) (Hansen et al., 2003). The weighting factors were set based on preliminary simulations to $w_1 = 6\times10^{-6}$; $w_2 = 1\times10^{1}$; $w_3 = 1\times10^{-1}$. Figure 5a illustrates the optical microscopy images of seed crystals, and Figure 5b presents the measured CLD (FBRM, Model D600), the estimated CSD and the simulated CLD corresponding to the estimated CSD. Off-line seed distribution analysis was intentionally avoided since that is not applicable *in-situ* for the NMPC experiments.

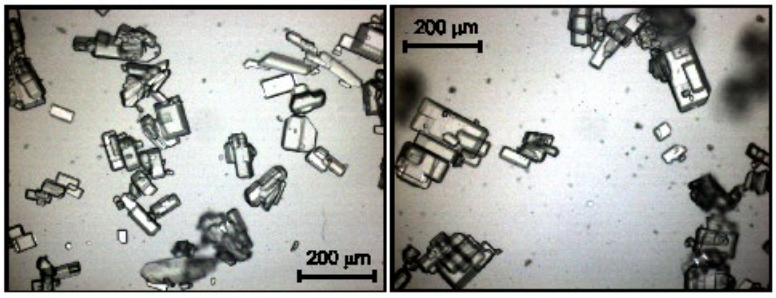


a)

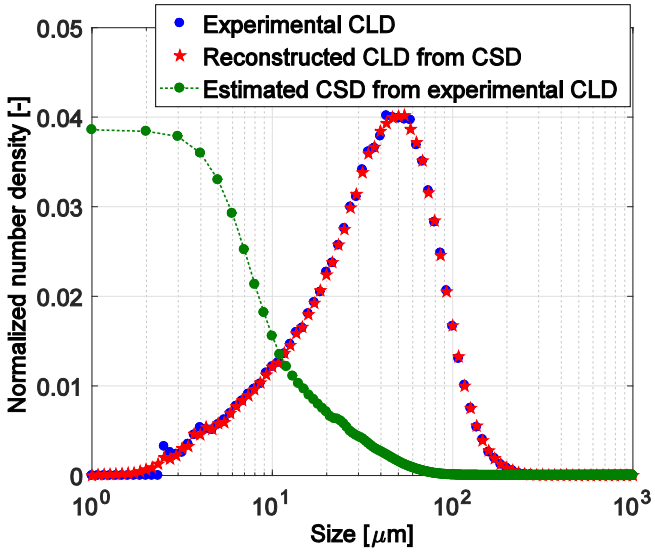


b)

**Figure 5**. a) Optical microscopy images of the seed crystals; and b) measured seed CLD, estimated seed CSD and the reconstructed CLD from the estimated CSD.

The estimation of kinetic parameters was carried out based on the concentration and CLD data from the experiments listed in Table 2, according to the following three main steps:

1. **PBM solution:** solution of model equations for the dynamic evolution of CSD and concentration.
2. **CSD to CLD forward transformation:** Application of the FBRM sensor model based on the CSD to CLD forward transformation to calculate the simulated CLD evolution.
3. **Parameter estimation:** Solution of the optimization problem to find the kinetic parameters by minimizing the deviation between the simulated and measured CLDs.

For proper scaling in the parameter estimation algorithm, the nucleation and growth rates were used in the following modified forms:

$$B(\sigma,T) = 10^{k_b'}\,\sigma^{b} V_C^{j} exp\left[-\frac{E_b}{RT}\right] \tag{11}$$

$$G(\sigma,T,L) = 10^{k_g'}\,\sigma^{g} L^{\gamma} exp\left[-\frac{E_g}{RT}\right] \tag{12}$$

The nucleation and growth rate constants of Eqs.(11)-(12) are set as exponents, thus they influence the kinetics on the same scale as the rest of the parameters. This transformation ensures the optimization process converges faster. The vector of kinetic parameters to be estimated is:

$$KP = \left[k_b'; b; j; E_b; k_g', g, \gamma; E_g\right] \tag{13}$$

The least-squares objective function used in the parameter estimation is expressed as:

$$OF(KP) = \sum_{i=1}^{K}\left|\frac{c_{m,i} - c_{s,i}}{c_{m,i}}\right| + w_1 \sum_{i=1}^{K}\sum_{j=1}^{M}\left|\frac{CL_{i,j,m}^{nw} - CL_{i,j,s}^{nw}}{CL_{i,j,m}^{nw}}\right| \tag{14}$$

The first part of the objective function fits the concentration, whereas the second part the non-weighted CLDs, in all available time moments ($K$) and CL bins ($M$). In the optimization $w_1$ was set to $3\times10^{-4}$. The optimization problem is then solved

$$\min_{KP} OF \tag{15}$$

using the CMA-ES global optimization algorithm (Hansen et al., 2003) from MATLAB R2015b.

Figure 6 presents the evolution of the measured and simulated concentrations and CLD during the batch corresponding to experiment 4 from Table 2. Here the concentration plot also illustrates well

the crystallization properties of L-ascorbic acid, indicating that high initial supersaturation is needed even for the secondary nucleation. Similar trends can be observed in the simulated and measured CLD data, too, indicating a good predictive ability of the model.

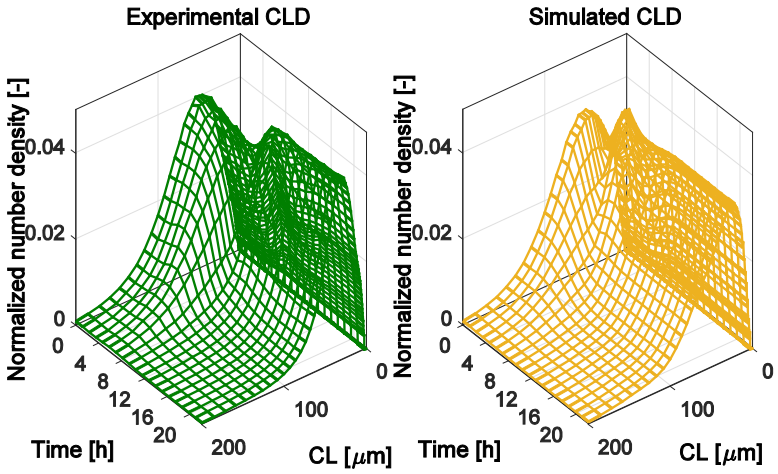


a)

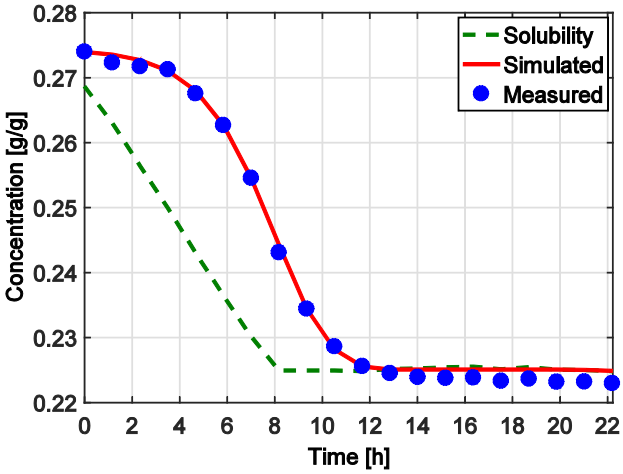


b)

**Figure 6**. Results of the model identification: a) simulated and measured CLD variations; and b) concentration variations during the same batch.

Table 4 presents the values of the estimated kinetic parameters and the bounds of the 95 % confidence intervals. The confidence intervals are narrow for each parameter, which suggests that all parameter are required in the model and are estimated with high reliability. The estimated growth rate constant might appear unrealistically high, however this compensates the high activation energy of growth, due to which the Arrhenius term has small value. The nucleation rate supersaturation exponent ($b$) is larger than the growth exponent ($g$), which is in good agreement with the experimental observations (Mersmann, 2001). The crystal volume dependence of secondary nucleation rate is relatively high (1.44). This is also in good agreement with the experimental observation that the seed crystals (lower solid fraction) initially generate lower secondary nucleation rate than later in the batch when the crystal volume is larger.

**Table 4**. The estimated nucleation and growth rate parameters.

| Parameter | Value | Bounds of 95 % confidence interval | |
|---|---|---|---|
| $k_b$ | $3.47\times10^{9}$ | $1.79\times10^{9}$ | $5.13\times10^{9}$ |
| $b$ | 0.95 | 0.73 | 1.14 |
| $j$ | 1.44 | 1.40 | 1.48 |
| $E_b$ | 32000 | 9110 | 54893 |
| $k_g$ | $3.72\times10^{16}$ | $2.85\times10^{16}$ | $4.69\times10^{16}$ |
| $g$ | 0.82 | 0.61 | 0.99 |
| $E_g$ | 105084 | 84176 | 126420 |
| $\gamma$ | $8.02\times10^{-2}$ | $7.21\times10^{-2}$ | $8.93\times10^{-2}$ |

It should be highlighted that the CSD to CLD transformation is a first principle model of the FBRM sensor. However, this sensor model is not validated directly with respect to experimental data, and as a direct consequence, the kinetic parameters might be linked to the eventual offsets and errors of this transformation. In this context, this kinetic parameter estimation is not intended to replace a detailed kinetic investigation, but constitutes an integral part of the adequate process model of the predictive control system. In this sense, none of the components of the system are evaluated independently for accuracy, but the integrated control system, consisting the process model, sensor model, estimation and error correction as well as the control algorithm work together to provide a platform suitable for real time CLD control.

### *NMPC system for CLD control of L-ascorbic acid crystallization*

The idea behind model based control approaches is the use of process model in real time to optimize input control signal(s) with respect to the objective function subject to imposed constraints. Measured output data is processed by the state estimator, which estimates the unmeasurable system states, which is required as initial condition for the NMPC optimizations, and it also mitigates the effects of disturbances. The procedure is repeated in every discrete time step.

Figure 7 presents the schematic diagram of the monitoring and control system. The crystallizer is equipped with an ATR-UV/VIS spectrophotometer (Zeiss MCS621 UV-VIS) for concentration monitoring, a thermocouple for temperature and an FBRM (Mettler Toledo V4.3.377) for CLD measurement. The temperature is manipulated through a Huber (Ministat 230) thermo-regulator.

The temperature and concentration data are collected by an in-house developed software, the Crystallization Process Informatics System (CryPRINS or CryMOCO), whereas the CLD is collected via the iC FBRM (V4.3.377) software. The sensor model and control calculations were carried out in the MATLAB R2015b. The concentration and temperature data is imported to MATLAB R2015b. through shared file (read-write communication) from the CryPRINS, while the CLD is read from the UA-OPC server of the iCFBRM. The NMPC computes the next temperature profile and passes it on to CryPRINS, which implements it through the chiller. This is a hierarchical control system: the supervisory model based controller calculates the required temperature trajectory, whereas the subsidiary level thermo-regulator (cascaded PI controller) implements this temperature profile on the jacketed crystallizer.

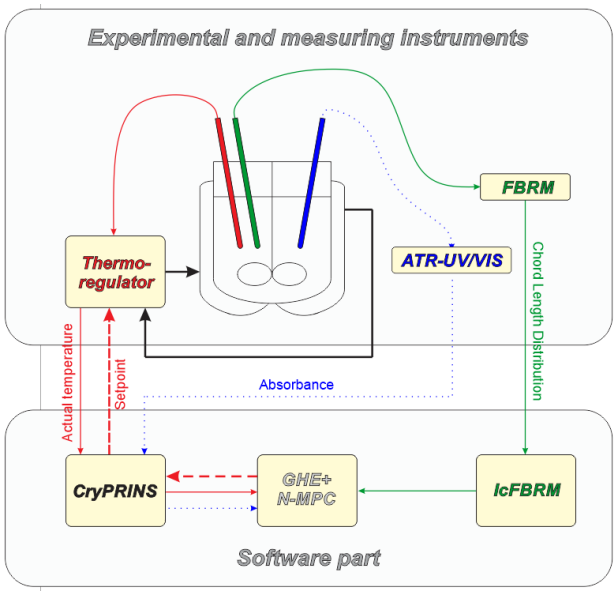


**Figure 7**. The schematic representation of the experimental setup, measurement instrumentation and software infrastructure.

The kernel of the model-based control system is the simulation of the process model and calculation of the optimal control moves. To improve the robustness of the control system, a growing horizon state estimator (GHE) was employed. The GHE uses the available measurements from the beginning of batch to the actual time to estimate the unmeasurable system states (CSD) for the NMPC optimization. In this system, the GHE also has the role to improve the model, as it also re-adjusts the crystallization kinetics based on the data gathered on the estimation horizon. This provides an adaptive feature of the algorithm and continuously improves the predictive power of the model.

Two popular dynamic optimization strategies are generally applied in NMPC calculations: direct single and direct multiple shooting approaches. The direct multiple shooting has considerably lower computational burden but it is much more sensitive to premature optimization stops (Mesbah et al., 2011a). Taking into account that high fidelity full PBE solutions are applied in both the GHE and the NMPC calculations, the probability of premature optimization stops is increased even with the more efficient multiple shooting techniques. For this reason, an accelerated single shooting method is employed in this work, namely the two-level repeated sequential optimization (RSO). The main idea of the RSO is to find a *crude* optimal temperature profile quickly then to refine it, with stronger emphasis on near-future temperature optimization, as presented in Figure 8. The performance and characteristics of this control system are described in more details in the literature (Szilagyi et al., 2018).

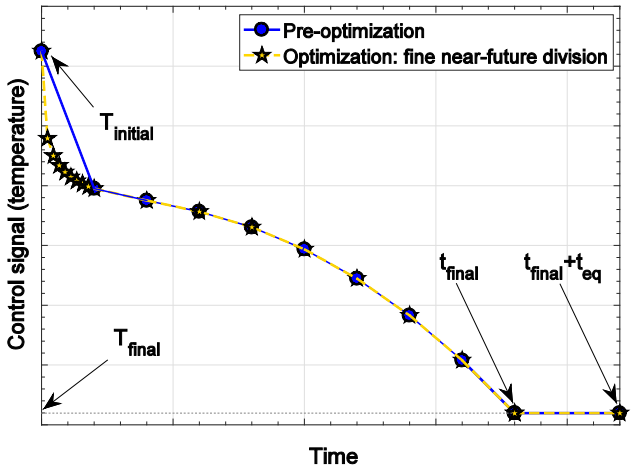


**Figure 8**. Representation of the two stage repeated sequential optimization algorithm.

In the NMPC optimization the following SSE based objective function is applied:

$$SSE(T_p) = \sum_{i=1}^{M} \left(CL_{i,sim} - CL_{i,ref}\right)^2 + w_1 \sum_{i=1}^{U} \left(T_{p,i} - T_{p,i-1}\right)^2 \quad (16)$$

where $T_p$ is the discrete temperature vector in the control horizon. The first part of the objective function ensures the desired product CLD, whereas the second part the smooth temperature profile. The variable $U$ is the length of the $T_p$ vector. The weighting factor was set to $w_1 = 1\times10^{-5}$. The optimization is carried out subject to the following constraints:

$$20 \leq T_{final} \leq 25 \text{ °C}$$

$$0.01 \leq c_r \leq 0.2 \text{ °C/min} \quad (17)$$

$$t_{eq} = 7200 \text{ s}$$

Where $c_r$ is the cooling rate and $t_{eq}$ is the equilibration time (until which the last temperature is kept after the end of temperature profile for desupersaturation).

Note that the target CLD is the measured CLD of a real crystal population. In this context, this NMPC is supposed to reproduce a realistic crystal population, which in practice could be the CLD fingerprint of the target batch. In this context, all batches controlled to the same final product CLD would be equivalent. This is a very advantageous operation mode of operation as the potential errors of the CSD to CLD transformations are completely omitted from the process control point of view. These might manifest only in the quality and value of the intermediate kinetic parameters.

The sum-squared error based objective function of the kinetic parameter (*KP*) readjustment, executed within the GHE on the estimation horizon is:

$$SSE(KP_{GHE}) = \sum_{i=1}^{Z}\left(c_{i,exp} - c_{i,sim}\right)^2 + w_1 \sum_{j=1}^{M}\sum_{i=1}^{Z}\left(CLD_{i,j,exp} - CLD_{i,j,sim}\right)^2 + w_2 \sum_{i=1}^{Z}\left(\aleph_{i,exp} - \aleph_{i,sim}\right)^2 \quad (18)$$

The first term of the objective function expresses the concentration, the second part the CLD and the third member represents the relative crystal number difference between the measured and simulated values. The weighting factors were set to: $w_1 = 2\times10^{-6}$; $w_2 = 2\times10^{-7}$. The variable $Z$ denotes the number of discrete time moments used in the state estimation (this is ***not*** necessarily equal to the number of available samples in the estimation horizon). The variable $\aleph$ is the normalized particle number; the simulated $\aleph_{sim}$ is the particle number normalized to the initial value, whereas the experimental $\aleph_{exp}$ is the FBRM count normalized to its initial value. The

optimization is carried out by using the *fmincon* MATLAB R2015b function with the interior point algorithm.

This NMPC implementation provides and exemplary case study for using a full PBM based adaptive-predictive control with growing horizon state and parameter estimation and sensor model incorporated in the algorithm. This approach shows excellent performance in controlling the CSD of L-ascorbic acid. Additionally, this study also serves as an experimental proof-of-concept and robustness test of the NMPC algorithm proposed in our recent work (Szilagyi et al., 2018), hence the approach was tested under more difficult process conditions and constraints imposed by realistic practical disturbances and uncertainties in the system:

- the seeds are added slightly above the (calculated) solubility concentration. However, the ascorbic acid might be partially oxidized thus this dosage can lead to partial seed dissolution and also measurement errors can occur.
- the seed loading is low (0.6 volume % of initial solution). For low seed loading the potential initial dissolution or eventual CLD measurement errors can generate considerable mismatch between the real and dosed quantity.
- relative short batch time is applied, namely 23 h, compared to the 96 h DNC time, pushing the process towards fast crystallization and potential nucleation events with uncertain kinetics.
- the initial parameter estimation and the NMPC experiments are carried out in two different crystallizers, using different agitator and FBRM probes, which might invalidate the estimated kinetic constants, used initially in the model, hence the adaptive feature of the proposed control system can be crucially important for the successful and robust control of the process.

Figure 9 summarizes the results of a typical NMPC experiment. Seed was introduced at time $t = 0$ and the NMPC started immediately. As it can be seen, the FBRM counts/s decreases at the beginning, indicating a partial seed dissolution. This might be caused by the preliminary oxidation of L-ascorbic acid and/or by the measurement inaccuracies. The natural reaction to the dissolution process is that the NMPC employs a quick cooling stage at the beginning. The fast initial cooling avoids the further dissolution. This is followed by a slow cooling period, giving time for the small seeds to grow. In this region, despite of the slow cooling, significant CL increase can be observed, which indicates considerable crystal growth, while the counts remain almost constant, thus there is no significant nucleation. The small increase in particle counts can also be explained by the presence of larger crystals, which also generate more CLs. However, due to the fixed batch time and hard constraint on crystallization yield the NMPC increases the cooling rate according to a typical parabolic cooling profile at the end of the batch to keep these constraints. This will lead to more nucleation as indicated by the increasing FBRM counts/s and the decrease in the mean CL. This nucleation could be minimized by allowing a longer batch time or compromising on crystallization yield.

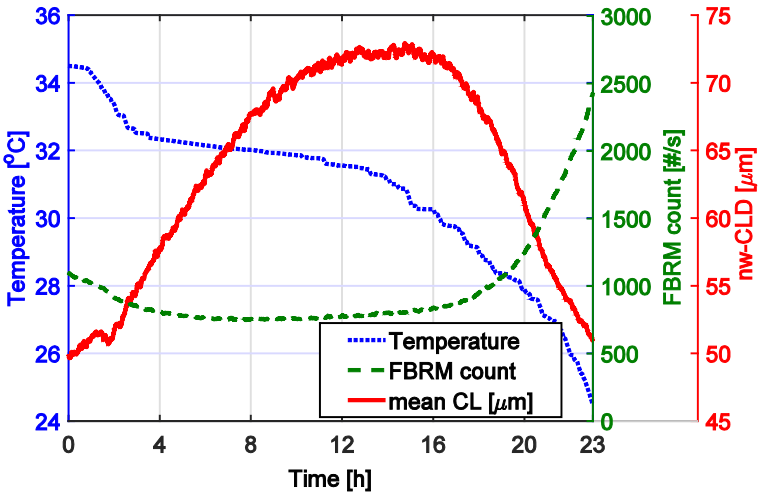


**Figure 9**. Summary of the results of a typical NMPC experiment: variation of FBRM counts/s, mean CL, and the temperature during the batch.

Nevertheless, the NMPC performed well from the point of view of robustness and optimality under these complex process conditions and considerable plant model mismatch (PMM). This experiment also suggests that including the dissolution kinetics in the model and allowing controlled dissolution might considerably improve the overall performance of the control by enabling fines dissolution, without extending the batch time or applying reduced temperature gradient.

Figure 10a illustrates the temporal variation of the CLD. The target CLD is closely achieved at the end of the batch. Although, as the upper view of the same surface (Figure10b) confirms, the most significant CLD variation is recorded in the slow cooling region, where the supersaturation is high and the seed crystals are growing fast.

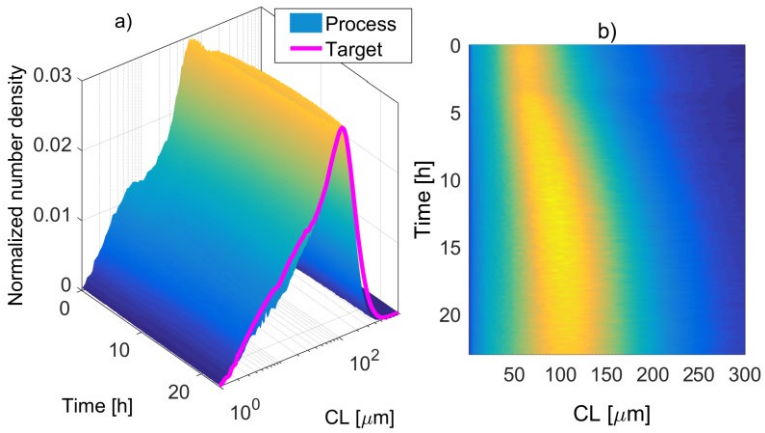


**Figure 10**. a) Variation of the CLD during the NMPC batch and the target CLD; and b) upper view of the CLD surface.

Figure 11 presents the phase diagram of the batch crystallization process as controlled by the NMPC. It can be seen that the process was conducted at approximately constant relative supersaturation ($c_s - c$), which resulted constantly increasing absolute supersaturation ($\sigma$). Note that no concentration data is available under 26 °C. This was because the ATR-UV/VIS system failed to record any data. However, the GHE was able to robustly handle this unexpected situation and the batch has been finished relying purely on the FBRM measurement. This indicates that the GHE system is extremely robust also against the temporary communication problems with the measurement devices, which would not be possible with the Kalman-filter based state estimators. This is due to the fact the GHE uses historical data from the entire batch run up to the current time step, from the beginning of the batch, which serves as known initial condition, whereas the other state estimation algorithms (such as extended Kalman filter) use only measurement available in the previous sampling step. This increased robustness of the proposed GHE becomes even more

important in industrial environment, as it can prevent the overall control system failure due to failures of the PAT tools or communication channels.

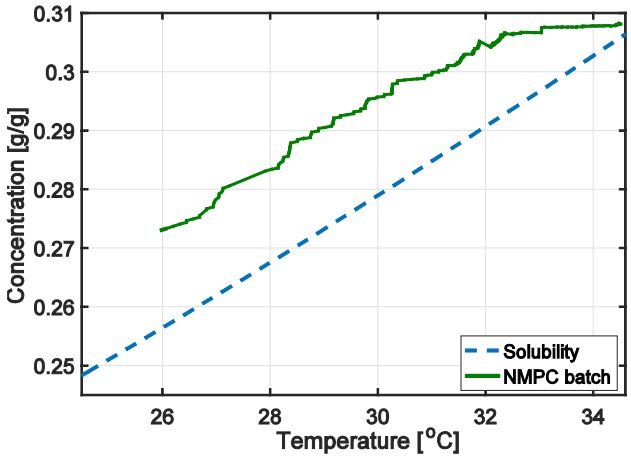


**Figure 11**. Operating trajectory during the NMPC batch in the temperature-concentration phase diagram.

Table 5 presents the initial and final kinetic parameters. According to the results presented in the table the GHE slightly readjusted the kinetic parameters. Nevertheless, due to the strong nonlinearity of the nucleation and growth rate functions, these slight variations might lead to large variations in the actual rates of nucleation and growth. Also, the values of final kinetic constants are in all case within the 95 % confidence intervals determined by the parameter estimation, except of the growth rate constant, which is slightly outside of the initial confidence range ($4.73\times10^{16}$ final value versus $4.69\times10^{16}$ upper bound of confidence interval) and size exponent of the growth rate ($9.68\times10^{-2}$ final value versus $8.93\times10^{-2}$ upper bound of confidence interval). These results also illustrate the robustness of the CLD measurement driven parameter estimation method. It must be

highlighted that the final parameters provided by the GHE are not necessarily the true kinetic constants of the process, since these are used to absorb all PMMs and disturbances. However re-estimating the parameters leads to considerable improvement of the model prediction of the on-going batch experiment. Parameters used for calculating optimal profiles need to be based on the actual parameters during the batch operation, which might be significantly modified due to PMM (for example some impurity in the starting material which decreases the growth kinetics).

**Table 5**. Initial and final values of nucleation and growth rate parameters, as readjusted by the GHE during the batch.

| Parameter | Initial | Final |
|---|---|---|
| $k_b$ | $3.47\times10^{9}$ | $4.33\times10^{9}$ |
| $b$ | 0.95 | 0.908 |
| $j$ | 1.44 | 1.46 |
| $E_b$ | 32000 | 34500 |
| $k_g$ | $3.72\times10^{16}$ | $4.73\times10^{16}$ |
| $g$ | 0.82 | 0.76 |
| $E_g$ | 105084 | 91100 |
| $\gamma$ | $8.02\times10^{-2}$ | $9.68\times10^{-2}$ |

The PVM images in Figure 12 compare the product crystals resulting from the batches controlled by the NMPC and the corresponding linear cooling. According to the images, the NMPC produced larger crystals with less fines than the traditional linear cooling operation mode (with same initial and final temperatures and identical batch time). The linear cooling profile lead to practically to a

bimodal product CSD with significant amount of fines. Therefore, the fine population can hardly be eliminated by dissolution, without dissolving significant part of the large fraction, too. In the NMPC product images the fines produced during the final stage of the batch, where more aggressive cooling was applied (see Figure 10), can be identified. Although, the NMPC might detect the nucleation and creates conditions, which favors the growth over nucleation, since heating was not allowed during the optimization of the temperature profile, these fine particles cannot be eliminated.

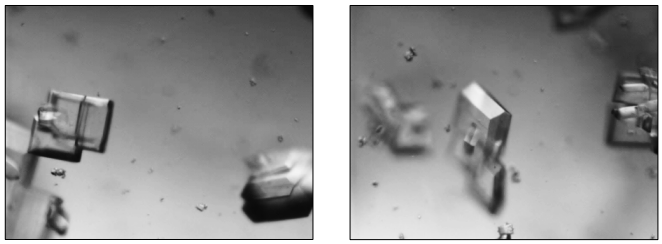

a)

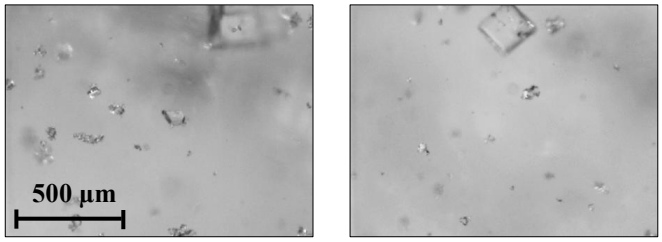


b)

**Figure 12**. PVM images of L-ascorbic acid crystals produced in the a) NMPC; and b) corresponding linear batch cooling experiment.

## Conclusions

Two Quality-by-Control (QbC) approaches for the batch cooling crystallization of L-ascorbic acid were analyzed in this work. First, a model-free QbC based on direct nucleation control (DNC) was

applied as a quick crystallization design approach via feedback control. The DNC however provided oscillatory control performance due to the particular crystallization kinetics of the systems, which introduces an apparent time delay in the nucleation rate during the cooling stages. Despite the oscillatory control the crystal quality was relatively good, but the batch duration was excessively long.

To reduce the batch time and overcome the process nonlinearity and apparent time delay, a model-based QbC approach was implemented based on an advanced model-based control, the nonlinear model predictive control (NMPC). In contrast with the DNC, the NMPC requires exhaustive system information and a suitable process model. A PBM was developed involving secondary nucleation and size dependent growth and it was solved with high accuracy using a HR-FVM. The kinetic parameters were estimated based on concentration and CLD data, involving a projection based real time CSD to CLD transformation. The estimated constants have realistic values and are estimated with narrow confidence interval bounds. The calibrated model simulates well the dynamic variation of concentrations and CLDs. For increased robustness of the approach the kinetic parameters were re-estimated during the NMPC experiment by a model based growing horizon state and parameter estimator. The proposed adaptive-predictive NMPC proved to be highly robust even under large plant model mismatch and sensor and/or communication failure. This work provides an exemplary case-study of the detailed implementation of a fully mechanistic PBM model based nonlinear predictive control framework, that incorporates PBM based prediction, real-time state and parameter estimation, real-time optimization as well as a sensor (FBRM) model that enables the model based design of optimal cooling profiles in batch crystallization. The approach was demonstrated experimentally for the crystallization of L-ascorbic acid from water providing very robust control even under large plant model mismatch

conditions. The results, and control performance in this system could be further improved by incorporating the dissolution mechanism in the model and enabling the heating (fines dissolution) in the NMPC optimizations. The proposed model-based QbC framework is generic and can be applied for the real-time model based design of most batch cooling crystallization systems.


## Acknowledgements

The financial support of the International Fine Particle Research Institution is acknowledged gratefully. Funding from the European Research Council under the European Union's Seventh Framework Programme (FP7/2007-2013)/ERC grant agreement No. [280106-CrySys] is also acknowledged.


## List of notations

$E_b$ - activation energy of nucleation [J mol$^{-1}$]

$E_g$ - activation energy of growth [J mol$^{-1}$]

$L_n$ - nucleon size [m]

$T_p$ - vector of temperatures in the prediction horizon [-]

$V_c$ - specific volume of crystals population [m$^3$ m$^{-3}$]

$c_r$ - cooling rate [$^o$C s$^{-1}$]

$k_b$ - nucleation rate constant [# m$^{-3}$s$^{-1}$]

$k_g$ - growth rate constant [m s$^{-1}$]

$p_i$ - solubility concentration [kg kg$^{-1}$]

$p_i$ - Solubility rate constant; i = 0,1,2 [kg kg$^{-1}$ $^{o}$C$^{-i}$]

$p_{ij}$ - Parameters of concentration calibration equation; i,j = 0,1,2 [kg kg$^{-1}$ A$^{-i}$ $^{o}$C$^{-j}$]

$t_{eq}$ - equilibration time [s]

$A$ - UV-VIS absorbance [-]

$B$ - nucleation rate function [# m$^{-3}$]

$b$ - supersaturation exponent of nucleation rate function [-]

$c$ - solute concentration [kg kg$^{-1}$]

$G$ - growth rate function [m s$^{-1}$]

$g$ - supersaturation exponent of growth rate function [-]

$j$ - crystal volume exponent of nucleation rate function [-]

$k$ - actual discrete (time) moment [-]

$K$ - number of used time moments [-]

$L$ - linear crystal size [m]

$M$ - number of (used) CLD discretization points [-]

$N$ - mesh size in the HR-FVM solution [-]

$n$ - number density function [# m$^{-3}$]

$R$ - gas constant [J mol$^{-1}$ K$^{-1}$]

$t$ - time [s]

$T$ - temperature [$^{o}$C]

$U$ - length of $T_p$ vector [-]

$w$ - weighting factor [-]

$Z$ - number of data points used in state estimation [-]

**List of Greek letters**

$\gamma$ - size exponent of growth rate function [-]

$\delta$ - size exponent of growth rate function [-]

$\rho$ - density [kg/m$^3$]

$\sigma$ - absolute supersaturation [-]

א - normalized particle number/FBRM count [-]

**Abbreviations**

*CL* - Chord Length

*CLD* - Chord Length Distribution

*CryPRINS* - Crystallization Process Informatics System

*CSD* - Crystal Size Distribution

*DNC* - Direct Nucleation Control

*FBRM* - Focused Beam Reflectance Measurement

*HR-FVM* - High Resolution Finite Volume Method

*IA-DNC* - Image Analysis based Direct Nucleation Control

*MPC* - Model Predictive Control

*NMPC* - Nonlinear Model Predictive Control

*OF* - Objective Function

*PAT* - Process Analytical Technology

*PB* - Population Balance

*PBE* - Population Balance Equation

*PBM* - Population Balance Model

*PDE* - Partial Differential Equation

*PMM* - Plant-Model Mismatch

*PVM* - Process Vision Microscopy

*GHE* - Growing Horizon Estimator

*RSO* - Repeated Sequential Optimization

*SSC* - Supersaturation Control

*SSE* - Sum Squared Error

*UV-VIS* - Ultraviolet-Visible

## References

Aamir, E., Nagy, Z.K., Rielly, C.D., Kleinert, T., Judat, B., 2009. Combined Quadrature Method of Moments and Method of Characteristics Approach for Efficient Solution of Population Balance Models for Dynamic Modeling and Crystal Size Distribution Control of Crystallization Processes. Ind. Eng. Chem. Res. 48, 8575–8584. https://doi.org/10.1021/ie900430t

Abu Bakar, M.R., Nagy, Z.K., Saleemi, A.N., Rielly, C.D., 2009. The impact of direct nucleation control on crystal size distribution in pharmaceutical crystallization processes. Cryst. Growth Des. 9, 1378–1384.

Acevedo, D., Tandy, Y., Nagy, Z.K., 2015. Multiobjective Optimization of an Unseeded Batch Cooling Crystallizer for Shape and Size Manipulation. Ind. Eng. Chem. Res. 54, 2156–2166. https://doi.org/10.1021/acs.iecr.5b00173

Agachi, P.S., Cristea, M.V., Nagy, Z.K., Imre-Lucaci, A., 2007. Model based control: case

studies in process engineering. John Wiley & Sons.

Agimelen, O.S., Hamilton, P., Haley, I., Nordon, A., Vasile, M., Sefcik, J., Mulholland, A.J., 2015. Estimation of particle size distribution and aspect ratio of non-spherical particles from chord length distribution. Chem. Eng. Sci. 123, 629–640. https://doi.org/10.1016/j.ces.2014.11.014

Barrett, M., McNamara, M., Hao, H.X., Barrett, P., Glennon, B., 2010. Supersaturation tracking for the development, optimization and control of crystallization processes. Chem. Eng. Res. Des. 88, 1108–1119. https://doi.org/10.1016/j.cherd.2010.02.010

Berg, J.M., Tymoczko, J.L., Stryer, L., 2010. Biochemistry, Biochemistry textbook.

Beuzelin-Ollivier, M.G., Chevreux, B., Dalluege, M., Van Gelder, M., Goese, M.G., Hauk, C., Koekman, B.P., Lee, C., Mayer, A.F., Meury, A., others, 2012. Fermentative vitamin C production.

Borsos, A., Szila, B., Agachi, P.S., Nagy, K., 2017. Real-Time Image Processing Based Online Feedback Control System for Cooling Batch Crystallization. https://doi.org/10.1021/acs.oprd.6b00242

Bötschi, S., Rajagopalan, A.K., Morari, M., Mazzotti, M., 2018. Feedback Control for the Size and Shape Evolution of Needle-like Crystals in Suspension. I. Concepts and Simulation Studies. Cryst. Growth Des. https://doi.org/10.1021/acs.cgd.8b00473

Eggers, J., Kempkes, M., Cornel, J., Mazzotti, M., Koschinski, I., Verdurand, E., 2009. Monitoring size and shape during cooling crystallization of ascorbic acid 64, 163–171. https://doi.org/10.1016/j.ces.2008.08.007

Griffin, D.J., Kawajiri, Y., Grover, M.A., Rousseau, R.W., 2015. Feedback control of

multicomponent salt crystallization. Cryst. Growth Des. 15, 305–317. https://doi.org/10.1021/cg501368y

Grosch, R., Briesen, H., Marquardt, W., Wulkow, M., 2007. Generalization and numerical investigation of QMOM. AIChE J. 53, 207–227. https://doi.org/10.1002/aic.11041

Gunawan, R., Fusman, I., Braatz, R.D., 2004. High resolution algorithms for multidimensional population balance equations. AIChE J. 50, 2738–2749. https://doi.org/10.1002/aic.10228

Hansen, N., Muller, S., Koumoutsakos, P., 2003. Reducing the time complexity of the derandomized evolution strategy with. citeseer.ist.psu.edu.

Hukkanen, E.J., Braatz, R.D., 2003. Measurement of particle size distribution in suspension polymerization using in situ laser backscattering. Sensors Actuators, B Chem. 96, 451–459. https://doi.org/10.1016/S0925-4005(03)00600-2

Hulburt, H.M., Katz, S., 1964. Some problems in particle technology. A statistical mechanical formulation. Chem. Eng. Sci. 19, 555–574. https://doi.org/10.1016/0009-2509(64)85047-8

Kacker, R., Salvador, P.M., Sturm, G.S.J., Stefanidis, G.D., Lakerveld, R., Nagy, Z.K., Kramer, H.J.M., 2016. Microwave Assisted Direct Nucleation Control for Batch Crystallization: Crystal Size Control with Reduced Batch Time. Cryst. Growth Des. 16, 440–446. https://doi.org/10.1021/acs.cgd.5b01444

Kail, N., Marquardt, W., Briesen, H., 2009. Estimation of particle size distributions from focused beam reflectance measurements based on an optical model. Chem. Eng. Sci. 64, 984–1000. https://doi.org/10.1016/j.ces.2008.10.039

LeVeque, R.J., 2002. Finite volume methods for hyperbolic problems. Cambridge university press.

Li, M., Wilkinson, D., Patchigolla, K., 2006. Obtaining particle size distribution from chord length measurements. Part. Part. Syst. Charact. 23, 170–174. https://doi.org/10.1002/ppsc.200601026

Ma, C.Y., Wang, X.Z., 2012. Closed-loop control of crystal shape in cooling crystallization of l-glutamic acid. J. Process Control 22, 72–81. https://doi.org/10.1016/j.jprocont.2011.10.007

Majumder, A., Kariwala, V., Ansumali, S., Rajendran, A., 2010. Fast high-resolution method for solving multidimensional population balances in crystallization. Ind. Eng. Chem. Res. 49, 3862–3872. https://doi.org/10.1021/ie9016946

McGraw, R., 1997. Description of Aerosol Dynamics by the Quadrature Method of Moments. Aerosol Sci. Technol. https://doi.org/10.1080/02786829708965471

Mersmann, A., 2001. Crystallization Technology Handbook. Marcel Dekker Inc., New York, Basel. https://doi.org/10.1080/07373939508917003

Mesbah, A., Huesman, A.E.M., Kramer, H.J.M., Nagy, Z.K., Van den Hof, P.M.J., 2011a. Real-time control of a semi-industrial fed-batch evaporative crystallizer using different direct optimization strategies. AIChE J. 57, 1557–1569. https://doi.org/10.1002/aic.12366

Mesbah, A., Huesman, A.E.M., Kramer, H.J.M., Van den Hof, P.M.J., 2011b. A comparison of nonlinear observers for output feedback model-based control of seeded batch crystallization processes. J. Process Control 21, 652–666. https://doi.org/10.1016/j.jprocont.2010.11.013

Mesbah, A., Kramer, H.J.M., Huesman, A.E.M., Van den Hof, P.M.J., 2009. A control oriented study on the numerical solution of the population balance equation for crystallization processes. Chem. Eng. Sci. 64, 4262–4277. https://doi.org/10.1016/j.ces.2009.06.060

Mesbah, A., Nagy, Z.K., Huesman, A.E.M., Kramer, H.J.M., Van Den Hof, P.M.J., Hof, P.M.J.

Van den, 2012. Nonlinear Model-Based Control of a Semi-Industrial Batch Crystallizer Using a Population Balance Modeling Framework. IEEE Trans. Control Syst. Technol. 20, 1188–1201. https://doi.org/10.1109/TCST.2011.2160945

Moldoványi, N., Lakatos, B.G., Szeifert, F., 2005. Model predictive control of {MSMPR} crystallizers. J. Cryst. Growth 275, e1349–e1354. https://doi.org/http://dx.doi.org/10.1016/j.jcrysgro.2004.11.170

Myerson, A.S., 2002. Handbook of Industrial Crystallization, Handbook of Industrial Crystallization. Elsevier. https://doi.org/10.1016/B978-075067012-8/50002-1

Nagy, Z.K., Braatz, R.D., 2012. Advances and New Directions in Crystallization Control. Annu. Rev. Chem. Biomol. Eng. 3, 55–75. https://doi.org/10.1146/annurev-chembioeng-062011-081043

Nagy, Z.K., Braatz, R.D., 2003. Robust nonlinear model predictive control of batch processes. AIChE J. 49, 1776–1786. https://doi.org/10.1002/aic.690490715

Nagy, Z.K., Fevotte, G., Kramer, H., Simon, L.L., 2013. Recent advances in the monitoring, modelling and control of crystallization systems. Chem. Eng. Res. Des. 91, 1903–1922. https://doi.org/10.1016/j.cherd.2013.07.018

Pappenberger, G., Hohmann, H.-P., 2014. Industrial production of L-ascorbic Acid (vitamin C) and D-isoascorbic acid. Adv. Biochem. Eng. Biotechnol. 143, 143–88. https://doi.org/10.1007/10_2013_243

Paz Suárez, L.A., Georgieva, P., Feyo de Azevedo, S., 2011. Nonlinear MPC for fed-batch multiple stages sugar crystallization. Chem. Eng. Res. Des. 89, 753–767. https://doi.org/10.1016/j.cherd.2010.10.010

Porru, M., Özkan, L., 2017. Monitoring of Batch Industrial Crystallization with Growth, Nucleation, and Agglomeration. Part 2: Structure Design for State Estimation with Secondary Measurements. Ind. Eng. Chem. Res. 56, 9578–9592. https://doi.org/10.1021/acs.iecr.7b00243

Qin, S.J., Badgwell, T., 2000. An overview of nonlinear model predictive control applications. Nonlinear Model Predict. Control 26, 369–392. https://doi.org/10.1007/978-3-0348-8407-5_21

Randolph, A., Larson, M., 1973. Theory of particulate processes. Academic Press, Salt Lake City.

Rawlings, J.B., Mayne, D.Q., 2012. Model Predictive Control: Theory and Design, Control. https://doi.org/10.1109/TBME.2009.2039571

Saleemi, A., Rielly, C., Nagy, Z.K., 2012. Automated direct nucleation control for in situ dynamic fines removal in batch cooling crystallization. CrystEngComm 14, 2196. https://doi.org/10.1039/c2ce06288g

Shalmashi, A., Eliassi, A., 2008. Solubility of L-(+)-ascorbic acid in water, ethanol, methanol, propan-2-ol, acetone, acetonitrile, ethyl acetate, and tetrahydrofuran from (293 to 323) K. J. Chem. Eng. Data 53, 1332–1334. https://doi.org/10.1021/je800056h

Simone, E., Zhang, W., Nagy, Z.K., 2015. Application of PAT-based feedback control strategies to improve purity and size distribution in biopharmaceutical crystallization, Cryst. Growth Des., 15 (6), 2908–2919. https:// 10.1021/acs.cgd.5b00337

Su, Q., Chiu, M. Sen, Braatz, R.D., 2017. Integrated B2B-NMPC control strategy for batch/semibatch crystallization processes. AIChE J. 63, 5007–5018.

https://doi.org/10.1002/aic.15810

Szilagyi, B., Agachi, P.S., Nagy, Z.K., 2018. Chord length distribution based modeling and adaptive model predictive control of batch crystallization processes using high fidelity full population balance models. Ind. Eng. Chem. Res. https://doi.org/10.1021/acs.iecr.7b03964

Szilágyi, B., Nagy, Z.K., 2016. Graphical Processing Unit (GPU) Acceleration for Numerical Solution of Population Balance Models Using High Resolution Finite Volume Algorithm. Comput. Chem. Eng. 91, 167–181. https://doi.org/10.1016/j.compchemeng.2016.03.023

Uesaka, H., Kobayashi, R., 2002. Pattern formation in the crystallization of ascorbic acid, in: Journal of Crystal Growth. pp. 132–137. https://doi.org/10.1016/S0022-0248(01)01892-9

Wierzbowska, B., Hutnik, N., Piotrowski, K., Matynia, A., 2011. Continuous mass crystallization of vitamin C in L(+)-ascorbic acid - Ethanol - Water system: Size-independent growth kinetic model approach. Cryst. Growth Des. 11, 1557–1565. https://doi.org/10.1021/cg101521k

Wierzbowska, B., Piotrowski, K., Koralewska, J., Matynia, A., 2008. Size-dependent growth kinetics of vitamin C crystals in water solutions of L(+)-ascorbic acid with the addition of methanol and ethanol. Polish J. Chem. Technol. 10, 60–65. https://doi.org/10.2478/v10026-008-0015-5

Wierzbowska, B., Piotrowski, K., Koralewska, J., Matynia, A., Hutnik, N., Wawrzyniecki, K., 2008. Crystallization of vitamin C in a continuous DT MSMPR crystallizer - Size independent growth kinetic model approach. Cryst. Res. Technol. 43, 381–389. https://doi.org/10.1002/crat.200711075

Worlitschek, J., Hocker, T., Mazzotti, M., 2005. Restoration of PSD from chord length

distribution data using the method of projections onto convex sets. Part. Part. Syst. Charact. 22, 81–98. https://doi.org/10.1002/ppsc.200400872

Yang, Y., Song, L., Nagy, Z.K., 2015. Automated direct nucleation control in continuous mixed suspension mixed product removal cooling crystallization, Cryst. Growth Des., 15 (12), 5839–5848. https:// 10.1021/acs.cgd.5b01219

Zhang, G.P., Rohani, S., 2004. Dynamic optimal control of batch crystallization processes. Chem. Eng. Commun. 191, 356–372. https://doi.org/10.1080/00986440490272546